ΠΑΝΕΠΙΣΤΗΜΙΟ ΘΕΣΣΑΛΙΑΣ

ΣΧΟΛΗ ΘΕΤΙΚΩΝ ΕΠΙΣΤΗΜΩΝ

ΔΙΑΤΜΗΜΑΤΙΚΟ ΠΡΟΓΡΑΜΜΑ ΜΕΤΑΠΤΥΧΙΑΚΩΝ ΣΠΟΥΔΩΝ

ΠΛΗΡΟΦΟΡΙΚΗ ΚΑΙ ΥΠΟΛΟΓΙΣΤΙΚΗ ΒΙΟΙΑΤΡΙΚΗ

Ανά λυση Ηχητικών Σημάτων ως Μέθοδος Παρακολούθησης Βιομηχανικών Διεργασιών

Κωνσταντίνα Μαλαμούση

ΔΙΠΛΩΜΑΤΙΚΗ ΕΡΓΑΣΙΑ

Επιβλέπων

DR. Κωνσταντίνος Δελήμπασης

Λαμία, 2019

UNIVERSITY OF THESSALY

SCHOOL OF SCIENCE

INFORMATICS AND COMPUTATIONAL BIOMEDICINE

Acoustic Emission Monitoring Technology for Quality Improvement and Increased Operational Performance

Konstantina Malamousi

Master thesis

DR. Konstantinos Delibasis

Lamia

June 2019

ΠΑΝΕΠΙΣΤΗΜΙΟ ΘΕΣΣΑΛΙΑΣ

ΣΧΟΛΗ ΘΕΤΙΚΩΝ ΕΠΙΣΤΗΜΩΝ

ΔΙΑΤΜΗΜΑΤΙΚΟ ΜΕΤΑΠΤΥΧΙΑΚΟ ΠΡΟΓΡΑΜΜΑ ΠΛΗΡΟΦΟΡΙΚΗ ΚΑΙ ΥΠΟΛΟΓΙΣΤΙΚΗ ΒΙΟΙΑΤΡΙΚΗ

ΚΑΤΕΥΘΥΝΣΗ ……..

«ΥΠΟΛΟΓΙΣΤΙΚΗ ΙΑΤΡΙΚΗ ΚΑΙ ΒΙΟΛΟΓΙΑ»

Ανά λυση Ηχητικών Σημάτων ως Μέθοδος Παρακολούθησης Βιομηχανικών Διεργασιών

Κωνσταντίνα Μαλαμούση

ΔΙΠΛΩΜΑΤΙΚΗ ΕΡΓΑΣΙΑ

Επιβλέπων

DR. Κωνσταντίνος Δελήμπασης

Λαμία, 2019-06-18

«Υπεύθυνη Δήλωση μη λογοκλοπής και ανάληψης προσωπικής ευθύνης»

Με πλήρη επίγνωση των συνεπειών του νόμου περί πνευματικών δικαιωμάτων, και γνωρίζοντας τις συνέπειες της λογοκλοπής, δηλώνω υπεύθυνα και ενυπογράφως ότι η παρούσα εργασία με τίτλο [«τίτλος εργασίας»] αποτελεί προϊόν αυστηρά προσωπικής εργασίας και όλες οι πηγές από τις οποίες χρησιμοποίησα δεδομένα, ιδέες, φράσεις, προτάσεις ή λέξεις, είτε επακριβώς (όπως υπάρχουν στο πρωτότυπο ή μεταφρασμένες) είτε με παράφραση, έχουν δηλωθεί κατάλληλα και ευδιάκριτα στο κείμενο με την κατάλληλη παραπομπή και η σχετική αναφορά περιλαμβάνεται στο τμήμα των βιβλιογραφικών αναφορών με πλήρη περιγραφή. Αναλαμβάνω πλήρως, ατομικά και προσωπικά, όλες τις νομικές και διοικητικές συνέπειες που δύναται να προκύψουν στην περίπτωση κατά την οποία αποδειχθεί, διαχρονικά, ότι η εργασία αυτή ή τμήμα της δεν μου ανήκει διότι είναι προϊόν λογοκλοπής.

Ο/Η ΔΗΛΩΝ/-ΟΥΣΑ

Ημερομηνία

Υπογραφή

Ανά λυση Ηχητικών Σημάτων ως Μέθοδος Παρακολούθησης Βιομηχανικών Διεργασιών

Κωνσταντίνα Μαλαμούση

Τριμελής Επιτροπή:

Κωνσταντίνος Δελήμπασης

Χαράλαμπος Σανδαλίδης

Αθανάσιος Κακαρούντας

Acoustic Emission Monitoring of High Velocity Oxy/Fuel Thermal Spray Processes

Abstract

This work is to lay the ground for the development of a novel on-line, non-destructive monitoring technology for the low temperature thermal spray coating processes based on the airborne acoustic emission (AE) during spray. Numerical simulations were carried out to probe into the relationship between AE signals and thermal spray parameters as well as the condition of the spray torch. After preliminary CFD modelling, the AE was measured using a broadband piezoelectric AE sensor positioned near the torch and the results were compared with the model predictions. The results of this work demonstrate that acoustic signals contain detectable information associated with spray parameters such as operating pressure, powder feed rate and nozzle condition. The results show that AE analysis can be used reliably as a continuous on-line monitoring technique so that deviations from the optimum spraying conditions can be detected early and corrected promptly; greatly reducing product rejections and re-coating compared to post-spray quality check.

Table of Contents

Chapter 1

Introduction

1.1 Objectives and scope

Advanced control systems, based on MFC, PLC and PC´s as those used in thermal spraying equipment lead to reproducible primary input parameters (gas flow rates, pressures, feed rates, gun movement), but they are not technically capable of monitoring the variation of the coating quality resulting from permanent or sudden modifications and fluctuations in the system hardware. Nozzle wear, clogging, troubling in feeding lines, gas leaks, tube erosion, etc are not detectable by these systems but are extremely important for practical applications. These modifications in the spraying parameters can produce substantial variation in the quality of the coating microstructure. These differences in the quality can produce catastrophic failures or even life-threatening situations in critical components used by the aerospace sector. If an Acoustic Emission (AE) monitoring equipment is able to grasp the slightest deviation from the optimum spray conditions, occurring during spraying, then it is possible to stop the process whenever an abnormal change is recorded. This implies that the spraying parts can be saved and no extra time is needed to recover them. Listening to the spray process and interpreting the acoustic emissions is a simple and cost-effective solution which will be easy to use and adopt. The proposed monitoring technique will also assist the technicians on when to replace the worn parts of the thermal spraying gun. By monitoring the process noise “characteristics” it is also possible to readjust the thermal spraying parameters of worn guns.

At the moment, all spray monitoring systems are static and they cannot be used when the torch is in motion. As such, they can only provide stagnant diagnosis of the spray process which is rarely the case in commercial applications onto complex parts. The above mentioned unresolved technical issues in continuous monitoring of thermal spray processes have serious implications in global operations and quality assurance. Large enterprises operating globally

are challenged with shorter product lifecycles, globalization of operations, and demand to move more complex products to market faster while maintaining the highest quality standards. The key to success is not just producing better products faster and more efficiently, the first time around; It also depends on controlling a multitude of complex processes with precision and adaptation to ever-changing requirements. In a further embodiment of this concept would be possible to upload live and historic spray data to a database, thereby enabling issues that affect quality to be quickly identified and resolved centrally—even across global operations and into the supplier network.

This work therefore describes a method of analysing the sources of AE generated prior to single and continuous multilayer HVOF thermally sprayed particle impact onto the substrate. Hence, it gives a measurement of the torch behaviour (not a direct indication of the coating quality) which could not be monitored using conventional methods such as SprayWatch.

1.2 Research Methodology

To assess the feasibility of this approach, a Computational Fluid Dynamics model was developed early in the project aiming to simulate the gas flow and aeroacoustics of the process. The gas flow analysis revealed the strong influence that the PFR and SOD have on the gas dynamics of the HVOF torch. The initial results were acquired by conducting a basic aeroacoustics analysis. The power frequency spectrum during HVOF was identified and the distinguishable acoustic signatures were broadly categorised. The simulations revealed that the PFR and SOD dominant frequencies have their origin in different turbulent structures. As a consequence, the dimensionality of the problem is relatively low because the variables do not carry the same information. The decision to use a shallow neural network for process monitoring, that could benefit from this condition, was made based on the CFD preliminary

results. Under different conditions, a more sophisticated deep learning algorithm and a larger dataset, would be necessary to unveil the complex correlations hidden in overlapping data.

A series of experiments were then designed in an effort to create a clean dataset for artificial neural network (ANN) training. The selected target coating property in this study is the microhardness. Microhardness is a key coating property when high wear protection is required, however other properties such as porosity, corrosion, decarburisation and toughness may be equally important depending on the mode of operation. This approach could be applied to monitor these additional properties, provided that sufficient experimental data are available. The research approach flow chart is depicted in **Figure 1**. The ANN model development is summarised in **Figure 2**. The selection of inputs is a major first step towards a neural network with good generalisation ability and accuracy. Instead of using unfiltered data in the network, some data cleaning was performed aiming to improve the ANN training and testing accuracy. The first training dataset was devised under different PFR conditions and a fixed SOD. In this way the power frequencies that carry input information were correlated to different PFRs. The highly corelated power frequencies were prioritised for later use in the final model. The second training dataset was prepared by altering the SOD at a fixed PFR. Similarly, the highly corelated power frequencies were selected as primary input to the final model. Finally, six frequency ranges for the PFR and four for the SOD were selected leading to a total of 10 power frequencies in the dataset. These ten inputs to the ANN model were selected for continuous monitoring and their correlation to the coating microhardness was assessed. The selected inputs in the form of power frequency range, carry information related to the SOD and PFR. In this way the accuracy of the monitoring process can be maintained when the PFR and SOD are altered during spray.

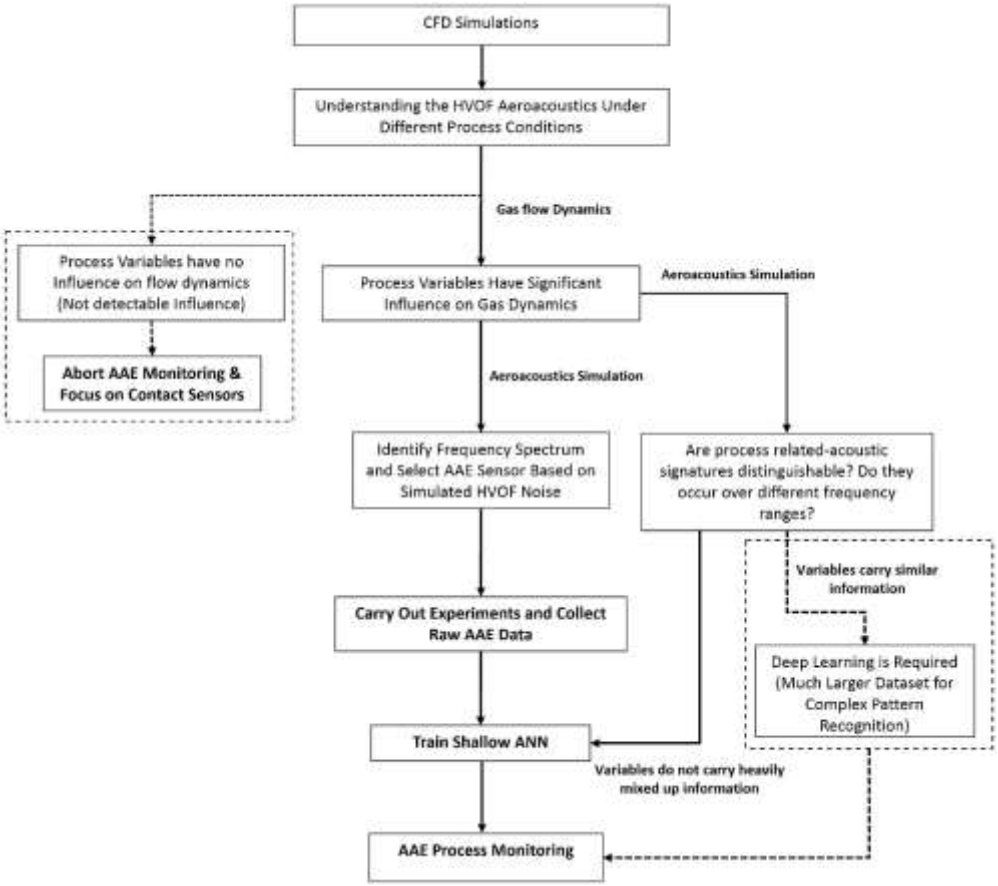

Figure 1. Research approach diagram

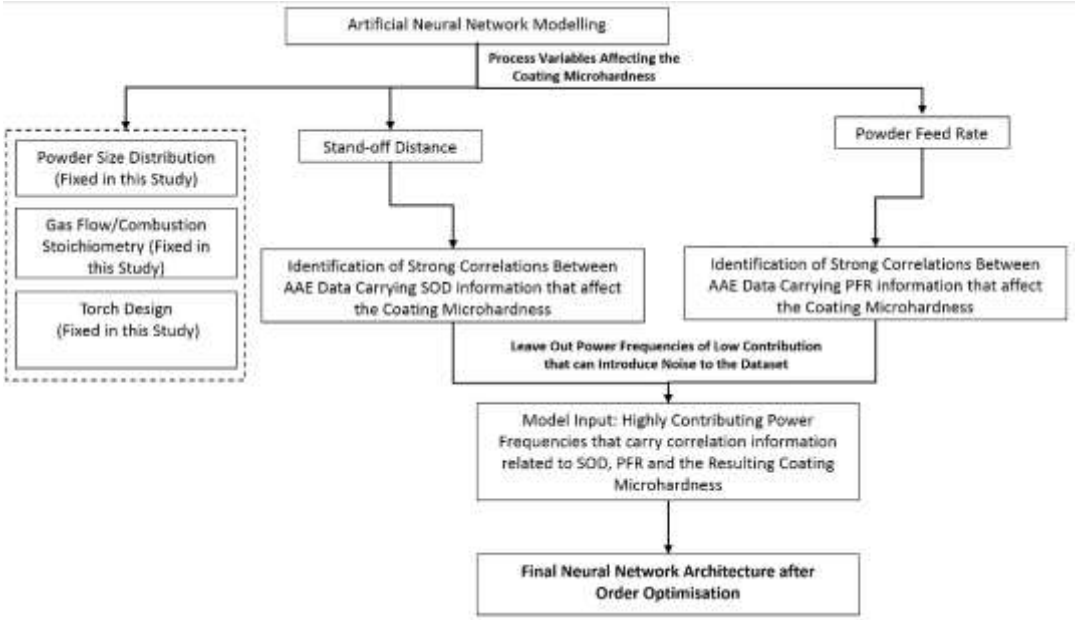

Figure 2. Artificial neural network model setup

1.3 Research Challenges

Thermal spray processes generate loud airborne noise from different sources in the spray booth. In this objective, it is critical to identify those sources and test different approaches of attaining the AE of interest with adequate accuracy and quality. The criterion to discriminate between different approaches will be the signal-to-noise ratio (SNR). Recent research has established the viability of successfully attaining the AE signal generated by impacting particles during thermal spray via contact PZT sensor. This task is far more challenging using an acoustic microphone due the high amplitude of the general airborne noise of the operation and the resulting reduction in the signal-to-noise ratio. Still the AE recording via acoustic means will be investigated due to the versatility and simplicity it would add to the final product (not having to attach a contact sensor on the sprayed part).

The modelling work is very demanding provided that a supersonic turbulent combustion models are solved simultaneously with the aeroacoustics and discrete phase equations. To achieve the desired computational outputs, an unsteady finite volume modelling approach using ANSYS Fluent subroutines has to be developed. The discipline of acoustics is intimately related to fluid dynamics. Many sounds that are technologically important in industrial applications are generated by and propagated in fluid flows. The phenomena associated with sounds can therefore be understood and analysed in the general framework of fluid dynamics. The main challenge in numerically predicting sound waves stems from the well-recognized fact that sounds have much lower energy than fluid flows, typically by several orders of magnitude. This poses a great challenge to the computation of sounds in terms of difficulty of numerically resolving sound waves, especially when one is interested in predicting sound propagation to the far field. Another challenge comes from the difficulty of

predicting the very flow phenomena (for example, turbulence) in the near field that are responsible for generating sounds. For predictions of mid- to far-field noise, the methods based on Lighthill's acoustic analogy offer viable alternatives to the direct method. In this approach, the near-field flow obtained from appropriate governing equations such as unsteady RANS equations, DES, or LES are used to predict the sound with the aid of analytically derived integral solutions to wave equations. The acoustic analogy essentially decouples the propagation of sound from its generation, allowing one to separate the flow solution process from the acoustics analysis. ANSYS Fluent offers a method based on the Fowcs-Williams and Hawkings (FW-H) formulation. The FW-H formulation adopts the most general form of Lighthill's acoustic analogy, and is capable of predicting sound generated by equivalent acoustic sources. ANSYS Fluent adopts a time domain integral formulation wherein time histories of sound pressure, or acoustic signals, at prescribed receiver locations are directly computed by evaluating corresponding surface integrals. Time-accurate solutions of the flow-field variables, such as pressure, velocity components, and density on source (emission) surfaces, are required to evaluate the surface integrals. Time-accurate solutions can be obtained from unsteady Reynolds-averaged Navier-Stokes (URANS) equations, large eddy simulation (LES), or detached eddy simulation (DES) as appropriate for the flow at hand and the features of interest (for example, vortex shedding). The source surfaces can be placed not only on impermeable walls, but also on interior (permeable) surfaces, which enables to account for the contributions from the quadrupoles enclosed by the source surfaces. Both broadband and tonal noise can be predicted depending on the nature of the flow (noise source) being considered, turbulence model employed, and the time scale of the flow resolved in the flow calculation. The FW-H acoustics model allows to select multiple source surfaces and receivers. Receivers can either be steady in the CFD reference frame or move with a user-specified constant velocity. The latter option enables modelling a "fly over"

situation. The model also permits either to save the source data for a future use, or to carry out an “on the fly” acoustic calculation simultaneously as the transient flow calculation proceeds, or both. Sound pressure signals thus obtained can be processed using the fast Fourier transform (FFT) and associated postprocessing capabilities to compute and plot such acoustic quantities as the overall sound pressure level (SPL) and power spectra. One important limitation of the integral FW-H formulation is that it is applicable only to predicting the propagation of sound toward free space. Thus, while the model can be legitimately used to predict far field noise due to external aerodynamic flows, such as the flows around ground vehicles and aircraft, it cannot be used for predicting the noise propagation inside ducts or wall-enclosed space.

Chapter 2
Literature Review

2.1 Existing HVOF Monitoring Techniques

At the moment, all spray monitoring systems (SprayWatch by Osier, Accuraspray by Tecnar and others) are static and they cannot be used when the torch is in motion. These systems are vital tools for design, process optimization and system calibration; However, can only provide stagnant diagnosis of the spray process which is rarely the case in commercial applications.

Existing process-monitoring technologies in HVOF focus on in-flight particle properties and characterisation of the gas jet by optical analysis. There are also systems to monitor substrate and coating temperature by infrared thermography as well as the thickness of each deposited layer of material.

Monitoring particle in-flight properties is achieved by one of two methods: single particle monitoring, or ensemble monitoring. The DPV 2000 monitoring system is a single particle system able to measure particle velocities, temperatures and diameters using a two-slit sensor head to measure radiation from particles with temperatures above 1000°C.

The velocity is obtained by measuring the time between the two signals which are triggered by a radiating particle passing the two-slit mask of the optoelectronic sensor head. Particle temperature is acquired by two-colour pyrometry, i.e., by calculating the ratio of the energy radiated at two different wave lengths assuming that the particles are grey body emitters with the same emissivity at both colour bands. The diameters are obtained from the radiation

energy emitted at one wavelength assuming that the melted particles are spherical or close to spherical. Since it is necessary to know the real emissivity of the particle a prior calibration by means of a powder with known diameter distribution has to be carried out. As the measurement volume is relatively small (<1 mm³) the data is collected for individual particles and can subsequently be analysed statistically. A certain measurement time is necessary to support the mean and standard deviations by a sufficient number of individual particle data.

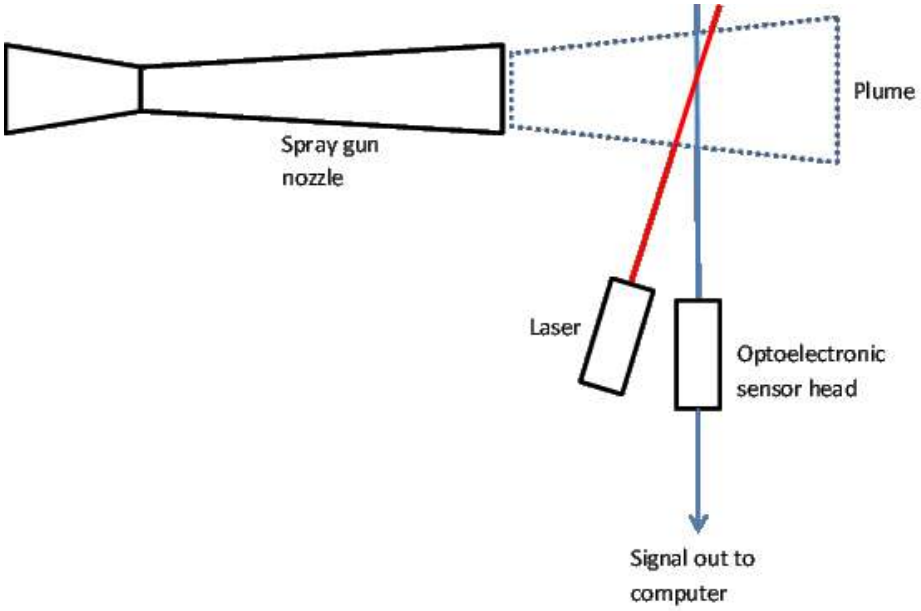

Figure 3 Simplified diagram of the DPV-2000 monitoring apparatus.

Contrary to the DPV-2000 the Spraywatch and Accuraspray-g3 diagnostic systems provide ensemble average data representing the particle characteristics in a measurement volume of approx. Ø 3 × 25 mm2. Particle velocities are obtained from cross-correlation of signals which are recorded at two closely spaced locations. The temperatures again are determined by two-colour pyrometry. As ensemble methods are used it is neither possible to evaluate the distribution and standard deviations of particle velocities and temperatures nor to estimate the particle diameters. The other component of these systems consists of a CCD camera enabling the analysis of the plume appearance (position, width, distribution, intensity).

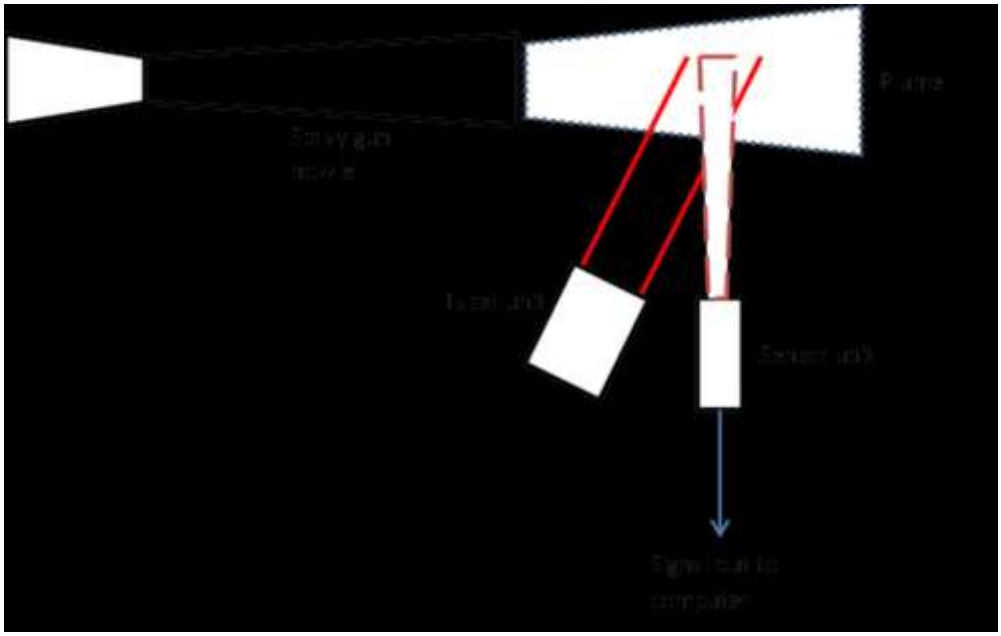

Figure 4 Simplified diagram of the Spraywatch monitoring apparatus.

2.2 Monitoring of HVOF Using Surface Contact Sensors

Research into acoustic emissions from the thermal spray process has primarily focused on the use of sensors in contact with the sprayed substrate to monitor the kinetic properties of particle deposition and the growth of coating defects such as cracks and delamination. For example, Faisal et al. [1] conducted successful experiments with a single contact sensor to measure the total kinetic energy of particles impacting the substrate. Crostack et al. developed a model relating velocity and diameter of particles to acoustic emission amplitude [2]. Lugscheider et al. investigated the relationship between spray angle and acoustic emissions [3]. Nishinoiri et al. used a non-contact laser AE technique to monitor the formation of defects such as microfracture and delamination in coatings [4]. These methods have shown promise in accurately monitoring the quality of thermal spray coatings as they are being sprayed, but the contact sensor must be carefully positioned on the substrate and calibrated for every part being sprayed. This drastically increases spraying time for each part and would necessitate training operators in the use of the monitoring equipment. These

studies rely on the Raleigh waves on the substrate surface due to particle impact, whereas the current investigation focuses on the airborne acoustic emissions (sound) produced during the HVOF process.

2.3 Welding Monitoring Using Acoustic Emissions Technologies

Airborne acoustic emissions studies for thermal spray process monitoring are very limited; However, in other processes such as various welding processes (VPPAW, SMAW, Laser Welding) and machining processes, acoustic emissions are closely monitored and analysed to give real-time predictions about certain aspects of the outcome of the process, or health of the hardware in use. This method has attracted considerable research interest. Studies show that the acoustic signal acquired during the welding process can be used to monitor weld characteristics, such as penetration quality [5, 6], weld pool status [7], irregularities and stability [8] during the welding process. Detection of defects by acoustic signal analysis is based on the identification of the acoustic characteristics and understanding of several phenomena, such as weld pool oscillation behaviour [9], arc plasma jet pulsation, change in arc intensity, and metal transfer, which are the relevant sources of sound generated during the welding process.

In the literature a variety of signal processing techniques, as well as neural networks and other methods, have been used to try and distinguish useful sound from background noise. Wang et al. [9] demonstrated the use of the short-time Fourier transform in detecting and locating irregularities on a weld bead. Wang and Zhao [5] used the variance of a segmented sound signal to monitor a keyhole opening. This feature was found to give a significant correlation with keyhole size, which can be utilized to monitor burn-through defects. Huang and Kovacevic [10] extracted the sound pressure deviation and band power from the acoustic signal and used them as the inputs of a neural network to establish the relation between

acoustic signal and depth of penetration in laser welding. Saad et al. [7] calculated the power spectral density of the segmented sound signal acquired from the welding process and used it as an input for a neural network model to distinguish the keyhole mode from the cutting mode. Grad et al. [8] found that kurtosis (sharpness of a peak of a frequency distribution curve) of acquired sound signals can be used to monitor the stability of a welding process.

2.4 Monitoring Machining Processes

Just like welding processes, skilled operators are able to identify tool wear and the occurrence of certain phenomena in many machining processes. Thus, acoustic emissions monitoring equipment and the use of signal processing methods such as neural networks should be able to identify these phenomena (and others beyond the range of human hearing) even more accurately, and without risk of harm to the operators hearing due to long durations of listening to a particularly loud process without hearing protection (i.e. ear defenders).

Microphones are a very suitable low-cost solution for chatter detection in milling, as their sensitivity to chatter onset is comparable to that of expensive contact-sensors such as plate dynamometers, displacement probes and accelerometers. This method is affected by some limitations (directional considerations, low-frequency response and environmental sensitivity) and for successful application, the suppression of environmental noise is imperative.

Tekıner and Yeşılyurt [17] used the sound signal to assess machinability of AISI 304 stainless steel, analysing the flank wear, built up edge, radii of chip curl, surface roughness and sound pressure. They measured and recorded sound pressure level (SPL) in the machining process and observed that it decreased with occurrence of chip removal. They affirmed also that measuring the cutting SPL is a suitable method for developing an alarm system.

Salgado and Alonso [18] highlighted that sound signal analysis during a cutting process has been used for a long time. In their study, they used Singular Spectrum Analysis to extract valuable information correlated with tool wear in the turning of AISI 1040 steel.

Samraj et al. [19] proposed an on-line measurement system, using Singular Value Decomposition of the emitted sound during the turning process, to estimate the flank wear of a tool. They used a microphone of 0.25" diameter with a dynamic range up to 122 dB with a frequency range of 20 Hz to 20 kHz. They found an increase in the SVD features as the tool flank wear increased, i.e., the condition monitoring of tool flank wear by emitted sound was proven possible and is a relatively simple process.

Lu and Wan [20] developed a method for tool wear monitoring in the micromilling of SK2 Steel using a microphone with bandwidth of up to 80 kHz (higher than the traditional microphone with bandwidth of up to 20 kHz). The collected signal was transformed to the frequency domain using Fast Fourier Transform (FFT) and applied to a Hidden Markov Model (HMM) neural network to process the signal and determine the tool condition.

A disadvantage of this method is that in the region between 0 and 2 kHz the influence of the surroundings and of the noise from adjacent machines, motors, conveyors, or processes can influence the signals [18]. This fact will be very important in our investigation. Moreover, frequencies below 100 Hz cannot be measured easily and the microphone tends to pick up high levels of background noise [21].

2.5 Thermal Spray and Sources of AAE

Thermal spraying encompasses a wide range of coating deposition processes with the common aspects that a feedstock, most commonly a powder, is partially melted by a supersonic flame (HVOF/HVAF) or plasma and propelled towards the substrate. These heated particles form splats on impact with the substrate and the coating is built layer by

layer. Important parameters of thermal spray processes include the powder feed rate, particle size, gas flow rates, fuel to oxygen ratio (in combustion thermal spray processes), nozzle geometry and stand-off distance. Changes in these parameters will mean changes in the resultant airborne AE, due to changes in energy from the system being transformed into the acoustic emissions. These are illustrated in the flowchart (**Figure 5)**. The flowchart illustrates that the variables which can potentially be monitored by AE combined with known parameters such as torch-movement will provide a good picture of the state of the process.

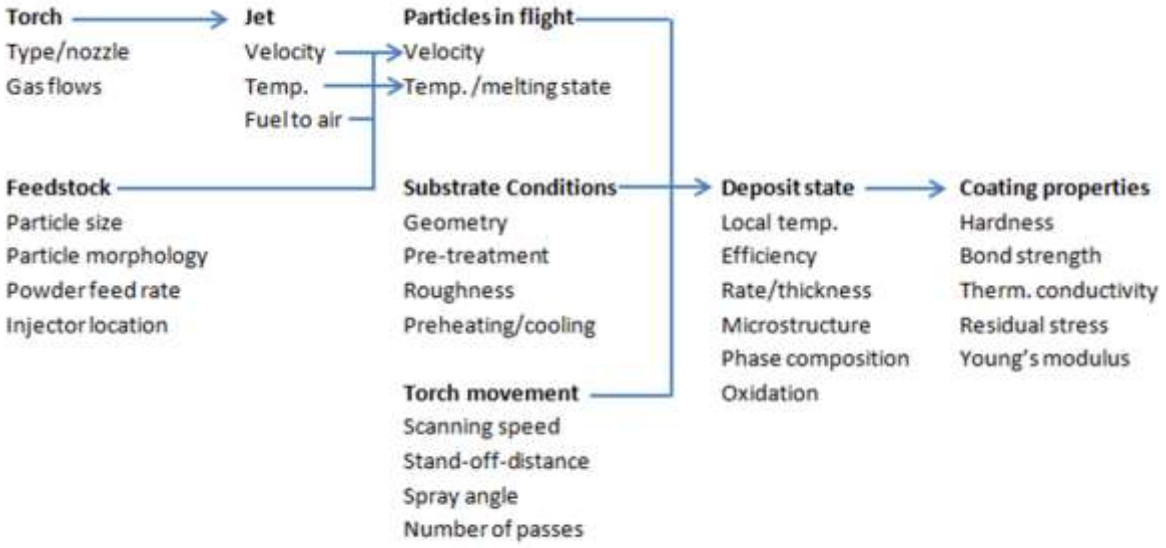

Figure 5 A linear flowchart demonstrating the interplay and interconnectivity of many of the controllable parameters of HVOF thermal spray.

The jet velocity fluctuations due to fluctuations in the combustion pressure are easily detectable due to overall decrease or increase of dB in the booth. In contrast, other process variables are more difficult to detect and classify. For example, increased or decreased powder feed rates, would mean more or less energy from the jet being transferred to the particles for their acceleration. These AAE variations are well hidden within a broad range of frequencies and their acoustic signature cannot be discovered effortlessly. Furthermore, due to thermo-mechanical induced stresses, the outlet diameter of a copper nozzle may increase

altering in this way the convergent-divergent pressure ratios and consequently altering the AAE signals. Regarding the supersonic jet noise itself, it can be monopole where there is fluctuation in mass flow, dipole on surfaces where the flow causes fluctuating pressure and quadrupole from turbulent wakes. In HVOF/HVAF supersonic jets, noise generated may be due to several reasons such as flow separation, incident turbulence, turbulent boundary layer and vortices in the wake region [11,12].

Chapter 3
Experimental and Numerical Methods

3.1 Acoustic Modelling of HVOF thermal spray process.

The studied spray torch is represented schematically in **Figure 6**. Fuel, Oxygen and Air are injected into the combustion chamber, where the fuel burns and the combustion products are accelerated downstream through the convergent-divergent nozzle. For the present analysis the nozzle configuration comprises of an inlet throat diameter of 5.5mm, 26 mm divergent length and outlet throat diameter of 7.5mm. Fine meshes are employed to the sensitive areas such as, the nozzle entrance and exit, the barrel exit and the free-jet centreline where high flow gradients are expected and increased accuracy is required. The governing equations of flow and acoustics are solved over the grid developed using the program Ansys FLUENT 19 Academic Edition [13]. The location of the sensor in the computational domain is shown in **Figure 6**. The same microphone location was used during the experimental acquisition of the acoustic signals. The coordinates from the nozzle exit are 0.055m (x), 0.025m (y) and 0m (z).

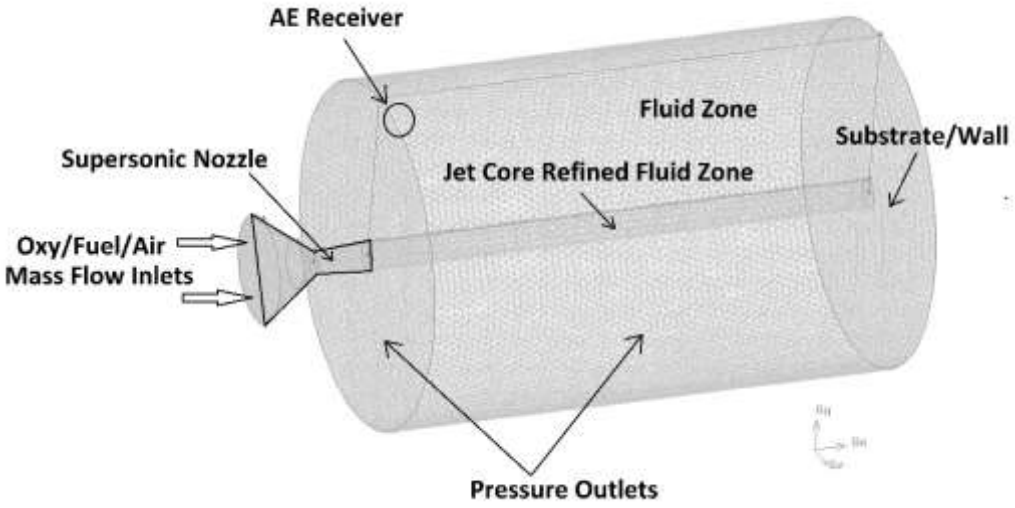

Figure 6. Computational fluid dynamics domain and boundary conditions

3.2 Solver Settings and Boundary Conditions

The phenomena associated with sounds can be understood and analysed in the general framework of fluid dynamics. ANSYS Fluent offers a method based on the Fowcs-Williams and Hawkings (FW-H) formulation [14]. The FW-H formulation adopts the most general form of Lighthill's acoustic analogy, and is capable of predicting sound generated by equivalent acoustic sources. The solver adopts a time domain integral formulation wherein time histories of sound pressure, or acoustic signals, at prescribed receiver locations are directly computed by evaluating corresponding surface integrals. It is out of this work's scope to probe into the mathematics of the modelling work. The authors have carried out extensive modelling and simulation work in the field of HVOF thermal spray and several validation data can be found in [11,12]. The detailed model setup parameters are summarized in **Table 1**.

Solver (Ansys 19)	3D-Transient	2nd order Explicit-Coupled, Compressible with a Fixed 10^{-7}-time step	Ref [12]

Turbulence	LES	Smarwoski-Lilly	Ref [15]
Combustion	Species/ Transport	Eddy-Dissipation	Ref [11,12,16]
Acoustics	FW-H	90^0 to Nozzle Exit	Ref [14]
DPM	Random Walk Model Particle Density: 5000 kg/m^3	Particle Size: 10x10^{-6} m	Ref [17,18,19]

Table 1. Aeroacoustics Model Setup

3.3. Neural Network Data Modelling

In their main embodiment Artificial Neural Networks are non-parametric methods used for pattern recognition inside large datasets. They generate an outcome based on a weighted sum of inputs which is afterwards passed through an activation function. The activation function defines the output from the neuron in terms of its combination. Three of the most used are the logistic, the hyperbolic tangent and the linear functions. In this study the logistic function has been used with a sigmoid shape. This activation is a monotonous crescent function which exhibits a good balance between a linear and a non-linear behaviour. A detailed description of perceptron theory, the main component of neural networks, can be found in the Neural Designer software online manual by Artificial Intelligence Techniques Ltd [20]. Of all artificial neural network types used in classification matters, a viable option is the multilayer perceptron (MLP) which is organized in three types of layers: an input layer, hidden layers (usually not more than three) and an output layer.

3.4 Artificial Neural Network Training

For this analysis a multilayer perceptron was used to model the AAE data from the HVOF process at Monitor Coatings-Castolin Eutectic in the UK. Although the number of hidden layers generally ranges between one and three, previous studies [21] have shown that ANNs with a single hidden layer can estimate any differentiable function, provided that they have

enough hidden units. Moreover, a high number of layers would significantly increase the processing time and the adjustments required during network training. The number of nodes in the hidden layer was varied between a minimum of three units and a maximum of 10 units. The analysis employed a total number of 10 input nodes corresponding to the spectral density of dominant frequencies when the spray distance and powder feed rate were altered during spray. The gas flows were fixed corresponding to maximum coating microhardness achieved at 100mm SOD and 1kg/h powder feed rate.

The weights were initialized using a uniform distribution within [-0.5, 0.5] range. Afterwards, these were adjusted using the gradient descent method with momentum rate and learning rate set equal to 0.1. The training was terminated when one of the stopping criteria was reached: A maximum number of 1000 of iterations and a variation in the average error below 0.001 for 10 consecutive cycles. The training was performed in a "batch" mode, meaning that weights were adjusted only after presenting all training records to the network. To reach a final approximation model, several cycles (epochs) were performed until meeting the aforementioned stopping conditions. Out of the 100 neural networks trained, the best in term of detection rates on the test set was retained. The selected neural network architecture shown in **Figure 7** is a multilayer perceptron (MLP 10-3-1) for the prediction of microhardness, containing 10 nodes in the input layer, 3 nodes in the hidden layer, and 1 output node. The evolution of the training set error was compared with the evolution of the validation error in order to make sure that the final model is not over-fitted, a characteristic that reduces the generalization capacity of the model when tested on new data. The ANN model setup is shown in **Table 2**.

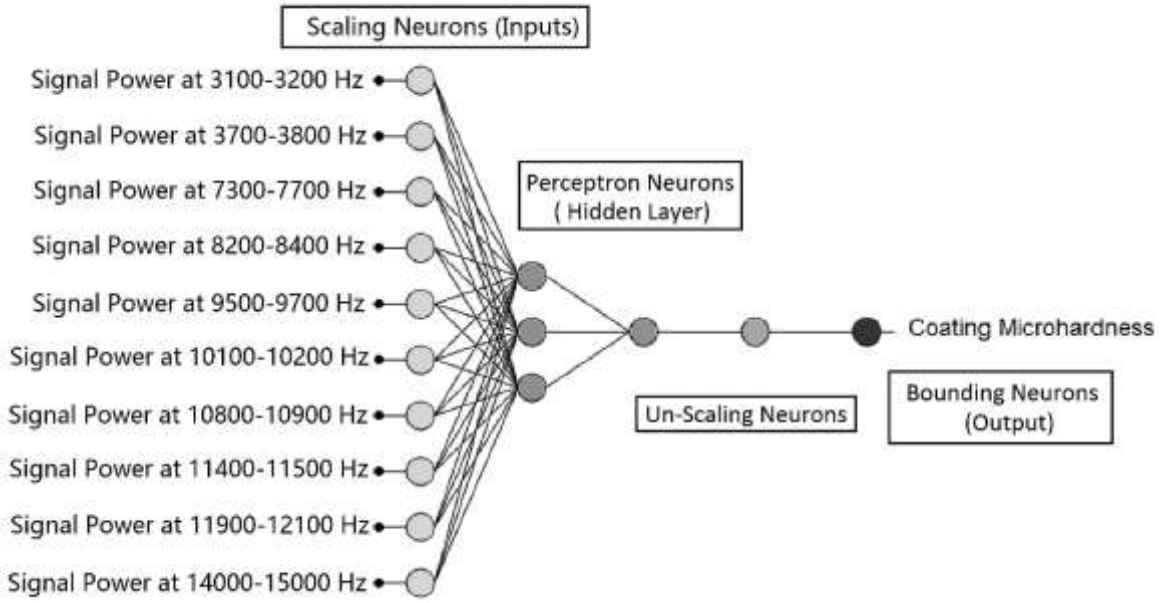

Figure 7. Neural network architecture used to predict the coating microhardness as a function of frequency power inputs

Scaling Method	Mean Standard Deviation [22]
Un-scaling Method	Mean Standard Deviation [23]
Bounding Layer	Yes
Error Method	Normalized squared error
Training Algorithm	Gradient Descent [22,23,24]
Activation Function	Hyperbolic Tangent [22]
Output Layer Function	Linear [22,23, 25]

Table 2. Artificial Neural Network model parameters

3.5 Experimental Apparatus

The acoustic emission monitoring apparatus comprises a single microphone with a preamplifier in an industrial thermal spray booth, a signal conditioning unit, and a PC for data

processing. The microphone was a 1/2" random incidence, high frequency, high amplitude, prepolarized microphone and preamplifier system. The microphone has a frequency range from 4Hz to 25kHz and distortion limit of 160dB with a noise floor of 19dBA. It was calibrated to compensate for the effect of its own presence in the acoustic field generated in the experiments. The microphone system was 77mm in length with a fitted grid of 13mm diameter, and was kept in a fixed position in the coating chamber behind a microphone windshield during spraying. The experiments were carried out using the above data acquisition setup **(Figure 8)** to monitor an HVOF system developed by Castolin Eutectic-Monitor Coatings Ltd in the UK [26,27].

A commercially available agglomerate sintered powder of WC- 17Co mass fraction (H.C Starck, AMPERIT 526) [27] was used for the deposition of coatings. The detailed chemical composition and size distribution of the powder are presented in [28]. The powder used shows the median size to equal about 18.9 μm. The measured particle size distribution ranges from 12.5μm – 28.1 μm at 10% and 90% of the cumulative respectively.

Figure 8. Signal acquisition unit and microphone used in this investigation by IFM electronics ltd.

The coatings were deposited onto steel substrates. The substrates where grit blasted with 46 μm alumina particles at a distance of 100 mm, subsequently they were blasted with high pressure air and mechanically cleaned to remove any remaining grit on the surface. The samples were sprayed using Castolin Eutectic-Monitor Coatings (UK) HVOF torch. The process parameters for the gun were previously optimised in-house using Oseir's SprayWatch system for achieving the best microstructure, the highest microhardness and optimum deposition conditions [26,27].

The experiments were performed with the HVOF gun traversing linearly over the substrates using a robotic arm. The spray angle was fixed at 90 degrees, while the SODs and powder feed rates were altered and individually controlled. This allowed for studying the influence of

each one on the generated acoustic signals inside the spray booth, while all other parameters were held constant. The increments in spray SODs were 100mm, 110mm,120mm, 130mm and 140mm. The powder feed rates were varying from 0.2kg/h to 2kg/h at 0.2kg/h increments for each individual SOD. Thus 50 combinations of SOD and PFR values were considered and an equal number of acoustic signals were acquired.

Post spray the samples were cut and polished following a routine developed to minimize and carbide pull-outs during polishing substituting the final stages of diamond polish with silica abrasive of 40 nm. Cross-sections of the samples were examined under the Optical Microscope at Monitor Coatings. The equipment is calibrated regularly as per Monitor's aerospace NADCAP accreditation requirements. The microhardness was examined with a Vickers micro indenter (Future Tech, FM-100) under a load of 300g (HV0.3). Ten measurements were taken per sample.

For the implementation of a prototype active monitoring system, it was decided that the unit should be able to notify the operator in real time. For this purpose, a preinstalled MATLAB application has been used in conjunction with the VSE001 (IFM electronics [29]) signal conditioning unit (**Figure 8**) to monitor the important frequency ranges that were identified and validated in the experimental program. These frequency ranges were used to set signal power thresholds which, when crossed, trigger an alarm suggesting a fault in the spray process.

Chapter 4
Results and Discussion

The modelling work focuses on the airborne acoustic signal acquisition when thermal spray powder is injected axially in the supersonic jet. High particle concentration in the flame results in strong coupling between the solid and fluid phases when the Strouhant number is >10. The flame temperature drops and the momentum transfer from the high energetic flame to the particles leads to jet velocity profile alteration both in the axial and the radial directions. It is expected these multiphase interactions to have an impact on the acoustic footprint of the process; However, it is unknown if the particle-flame interactions are detectable and over which frequency and spectral density range detection may occur. The underlying physics of this process are not well documented in the literature and our intention is to probe into this HVOF spray characteristic. In this study the aeroacoustics modelling work has been validated by comparing the experimental and modelling signal Fourier transforms.

4.1 Fluid flow and Aeroacoustics

The complicated structure of the supersonic jet [30] is shown in **Figure 9**. First, the jet boundary oscillates as the jet gas periodically over expands and converges in its attempt to match the ambient pressure. The gas continually overshoots the equilibrium position because the effects of the boundary are communicated to the interior of the jet by sound waves, which, by definition, travel more slowly than the bulk supersonic flow. The characteristic paths of the sound waves converge to form the second feature of the jet, the network of crisscrossed shock waves, or shock diamonds. These standing shocks alternate with rarefaction fans. The gas in the jet interior expands and cools down as it flows through the rarefaction fans and is

compressed as it passes through the shock diamonds. The jet structure shown in **Figure 9.a** and **9.b** in reality does not have sharp, stable boundaries but turbulent boundaries where jet and ambient gases mix. Near the orifice, where the pressure mismatch is large, Mach reflections occur but further downstream the reflections are regular. The mixing layer which grows eats its way into the supersonic core of the jet. When the mixing layer reaches the axis of the jet the flow is subsonic and fully turbulent. Large and small eddies are formed in the shear layer of the gas jet. These eddies are very small in size near the nozzle exit where they originally form, and then become larger downstream until full dissipation. Ultimately, the formation, propagation and dissipation of eddies result in the jet noise.

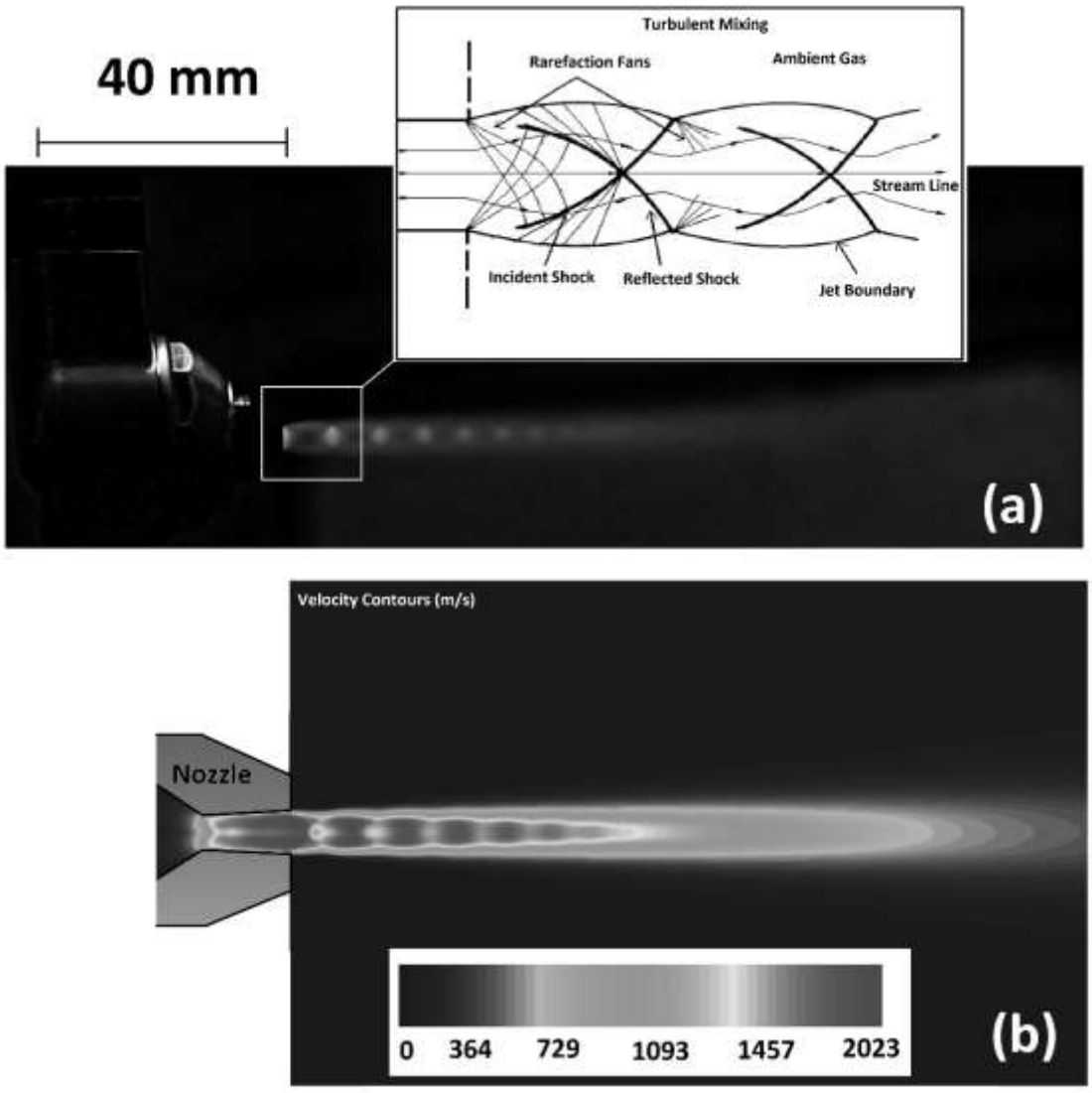

Figure 9. a) Image showing the experimental supersonic jet expansion b) Velocity contours of the simulated supersonic jet expansion

When the powder is introduced into the flame at 5kg/h feed-rate, the mean velocity profile is affected as depicted in **Figure 10**. To demonstrate this behaviour, we provide the evolution of the radial velocity profile of the gas in several different axial locations in the external flow field with and without powder in the jet. These locations are based on the distance from the exit of the HVOF torch. It is clearly seen that the centreline velocity decays along the axial direction faster in presence of the discrete phase and the jet propagates outwards in the radial direction (**Figure 10.b, d, e**). At larger standoff distance (x = 80mm from the nozzle exit), the velocity at the jet core is nearly half compared to the powder-free jet. Turbulent mixing with the ambient air occurs faster attributed to the jet kinetic energy being transferred to the particles during inflight acceleration. While the velocity slows down in the centreline, the boundaries of the jet are thrusted outwards as the flow is blocked by the particle cloud confined in the axis of the jet as shown in **Figure 10.a**. Several studies [31,32,33] have demonstrated the effect of supersonic jet diameter in the aeroacoustics. Typically, a wider jet creates a shift in frequencies where energy peaks occur. This is more evident in the high frequency range where the signal contribution originates form the small highly energetic turbulent eddies occurring near the nozzle exit at the jet-ambient gas boundary. The observed faster velocity dissipation is expected to alter the formation of large eddies downstream, contributing to the low frequency range as well. The modelling results suggest that an overall frequency shift of the noise peaks should be expected due to the particle laden flow in the jet and the consequent velocity profile alterations.

The Large Eddy Simulation predictions, coupled with the FW-H noise model approach (**Figure 11**), shows a similar trend as that measured experimentally. This means that the nature of the non-uniform quadrupole orientation is captured well by the CFD simulations.

The noise predictions are found to be in good, but not perfect, agreement with the experimental data. As expected, we have underpredicted the noise level at high frequencies. This is due to the small turbulent structures of the jet which are not resolved by our mesh. However, in general, the LES-FW-H approach demonstrates the ability to capture the spectra shape correctly. More specifically, the predicted power spectral density is lower in the low frequency range, higher in mid frequencies and lower over higher frequencies. The model accuracy can be improved by reducing the simulation time step, increasing the simulation overall time and by refining the mesh; However, this would require several months of computational effort since the aeroacoustics, turbulent combustion, compressible supersonic flow and discrete phases are solved simultaneously in a 3-D space.

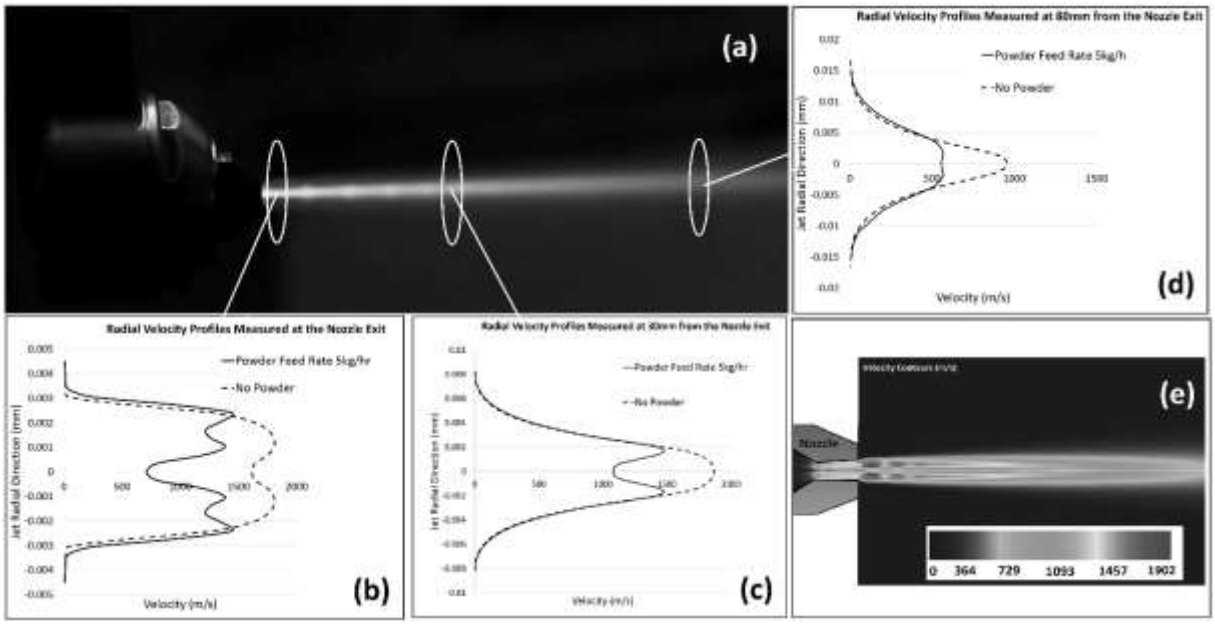

Figure 10. a) Image showing the powder travelling through the centreline of the supersonic jet, b) Radial gas velocity profile at the nozzle exit, c) Radial gas velocity profile 30mm downstream, d) Radial gas velocity profile 80mm downstream, e) Velocity contours with 5kg/h powder feed rate (Published Results [36])

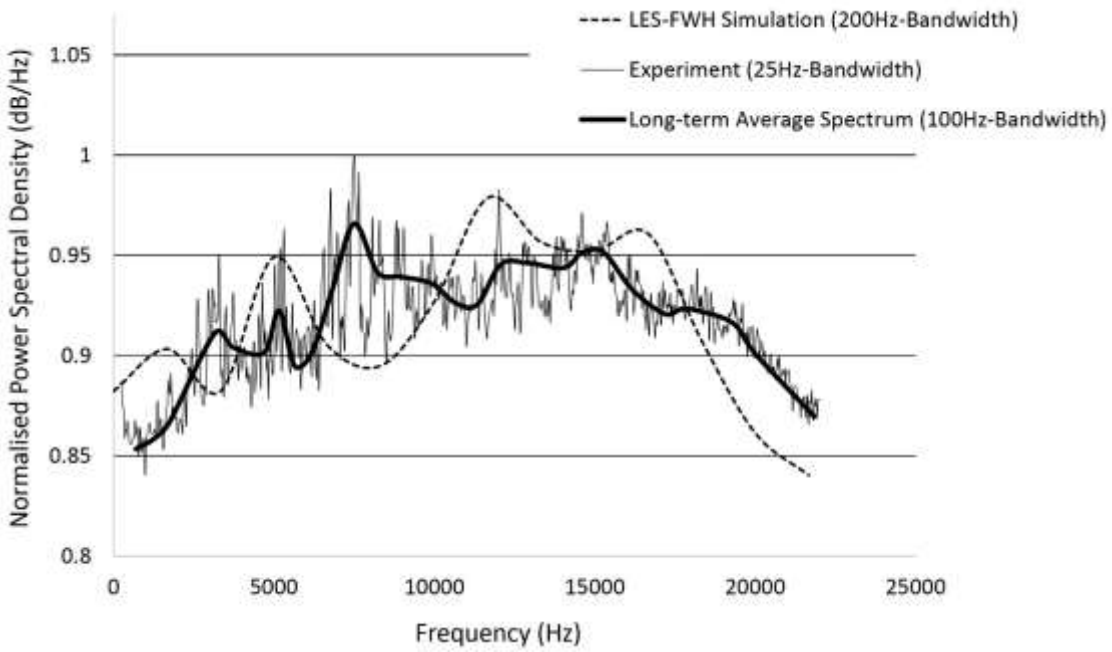

Figure 11. Time average Spectrogram showing the experimental and numerical noise acquisition without a substrate and powder in the flame. The bold solid line shows the experimental spectrogram after 100Hz bandwidth and 10 seconds time averaging. (Published Results [36])

A large amount of experimental evidence suggests that acoustic waves are strongly coupled to many mechanisms encountered in turbulent flows. The free shear layers are especially sensitive to acoustic waves [34]. This interaction may lead to large flow instabilities therefore it is important to avoid artificial free boundary reflection of the acoustic waves. To overcome this issue, we damp reflected waves by numerical viscosity, using a coarse mesh near the outlet boundaries (buffer zones). Although this approach is effective for the elimination of reflected waves, a coarse mesh may result in localized numerical resolution reduction

responsible for the over predicted noise at the very low frequency range as shown in **Figure 11**. Another distinctive feature of the process is the fragmentation of power peaks over a range of frequencies. At the early stages of this work the numerical approach revealed that we should be looking for energy-frequency pairs rather than maximum or minimum amplitude over the full range of frequencies. The same behaviour was later observed experimentally when the powder feed rates were altered from low (1kg/h) to high (4 kg/h) as shown in **Figure 12**. At high feed rates the power spectral density is lower over the frequency range up to 5,000 Hz. The peak power is observed at 15,000 Hz, while for the low powder loading occurs at 5,000 Hz. This is in line with the fluid flow (**Figure 10**) and aeroacoustics modelling results (**Figure 12**) suggesting a jet shape change due to faster decay of the jet core and the small jet diameter increase when powder is present in the flame. A clearer shift of the power peaks to the lower frequency range is observed when the jet hits a substrate at short standoff distances as shown in **Figure 13**. At 80mm from the nozzle tip, the jet experiences a rapid deceleration upon impact creating large circulation zones (vortex induced zone) near the substrate. These large turbulent structures give rise to the low frequency power spectrum. This effect dominates over the upstream shear layer mixing noise. Moving the substrate to 120mm from the nozzle allows for more canonical jet decay, where mixing layer structures at the mid frequency range dominate the noise generation process.

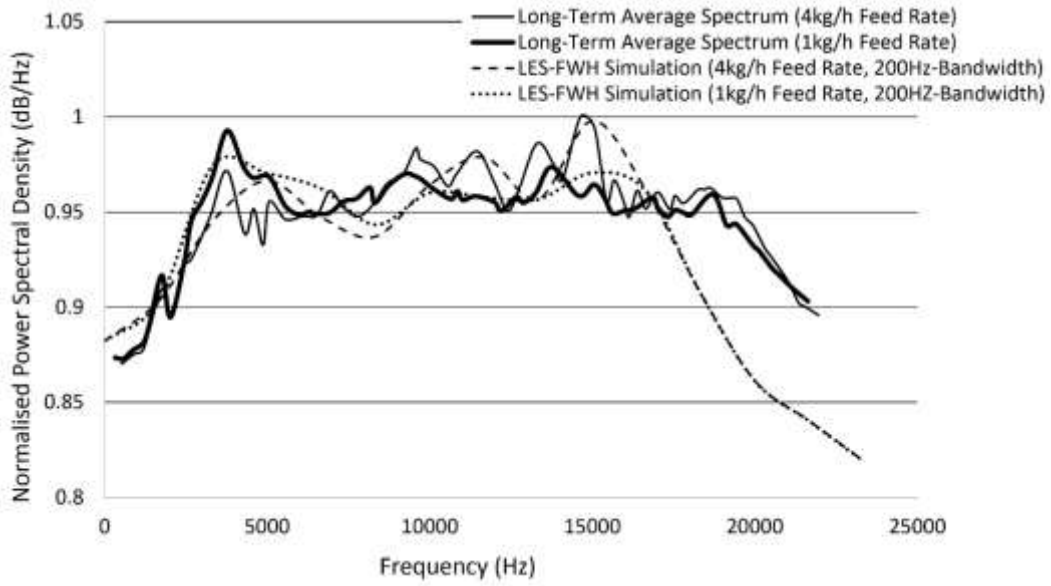

Figure 12. Time Average Spectrogram showing the experimental and numerical noise acquisition at different powder feed rates and without a substrate. Experimental spectrogram at 100Hz incremental bandwidth and 10 seconds time averaging. (Published Results [36])

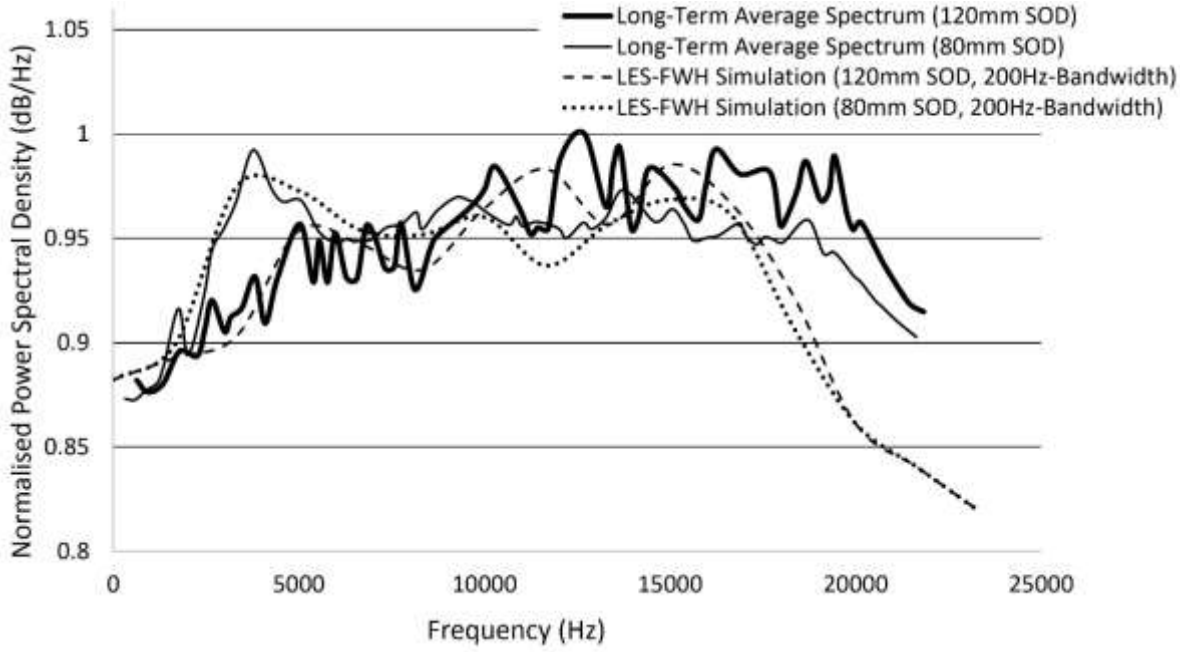

Figure 13. Time Average Spectrogram showing the experimental and numerical noise acquisition at different substrate standoff distances and fixed powder feed rate. Experimental spectrogram at 100Hz incremental bandwidth and 10 seconds time averaging. (Published Results [36])

When thermal spray phenomena are examined in isolation, the interpretation of the dataset is straightforward. However, the increased complexity of data handling and interpretation can be realized when the problem is grounded to reality where the above spray conditions are combined introducing variable SOD, feed rates and particle substrate impact noise to the spray process. A powerful instrument for disentangling the complexity of their subject matter is required, especially when we do not possess a clear knowledge of the dynamical relationships among these spray factors and the resulting acoustic signals. In this context, ANNs can help to identify the possible causes and their peculiar combination linked to the onset of a certain coating property by analysing the acoustic signals.

4.2 Experimental Acoustic Data Modelling

In this section we introduce a neural network model for the analysis of the experimental data with the aim of finding fundamental relationships between the target coating properties and the emitted acoustic signals during spray. The ten power frequency ranges shown in **Table 3** (Column 3 to Column 12) are the 10 down selected power frequencies as detailed in section 2 having had the leave-out technique applied and having discarded the unwanted frequencies. The feature vector comprises of 6 peak power frequencies highly corelated to PFR (3,100-3,200Hz, 14,000-15,000Hz, 3,700-3,800Hz, 7,300-7,700Hz, 10,100-10,200Hz & 10,800-10,900Hz) and 4 peak power frequencies carrying information predominantly for the SOD (8,200-8,400Hz, 7,300-7,700Hz, 11,900-2,100Hz, 9,500-9,700Hz,). The dataset of the 50 experiments/instances that were described in “Equipment and Experimental Process” was

randomly split into 40 training and 10 testing/validation dataset, of size equal to 40 and 10 respectively.

	Column 1	Column 2	Column 3	…….	Column 12	Column 13
Row 1	Powder Feed Rate (kg/hr)	Standoff Distance (mm)	Normalised Peak Power Spectral Density (dB/Hz) at Frequency Range 3000-3200Hz	…….	Normalised Peak Power Spectral Density (dB/Hz) at Frequency Range 14000-15000Hz	Coating Microhardness (HV0.3kg)
Row 2	0.2	100	0.36	…….	0.72	1300
Row 3	0.4	100	0.37	…….	0.68	1310
. . .	. . .	. . .	. . .	…….	. . .	. . .
Row 51	2	140	0.48	…….	0.99	1030

Table 3. Data matrix for developing the artificial neural network model.

4.2.1 Correlation ratios of PFR within the selected frequency bands

A training strategy was applied to the neural network in order to obtain the lowest possible loss. Loss value implies how well or poorly a certain model behaves after each iteration of optimization. The accuracy of a model is determined after the model parameters are learned. The test samples (data that were not used to train the ANN) are fed to the model and the number of mistakes the model makes are recorded, after comparison to the true values. Then the percentage of misclassification is calculated. The type of training is determined by the way in which the adjustment of the parameters in the neural network takes place. In this study the quasi-Newton method is applied to adjust the network weights in order to minimize the error (loss) function. This method is based on Newton's method, but does not require calculation of second derivatives, instead, it computes an approximation of the inverse Hessian at each iteration of the algorithm, by only using gradient information. As shown in **Figure 14.a** the initial value of the training loss was 13.8196%, and the final value after 333 iterations was 0.00501855%. The initial value of the validation loss was 15.0176%, and the final value after 333 iterations was 0.922464%. The very low validation error implies that the

model can generalise to unseen data and can distinguish between PFR and SOD contributions when the information coexist in the dataset.

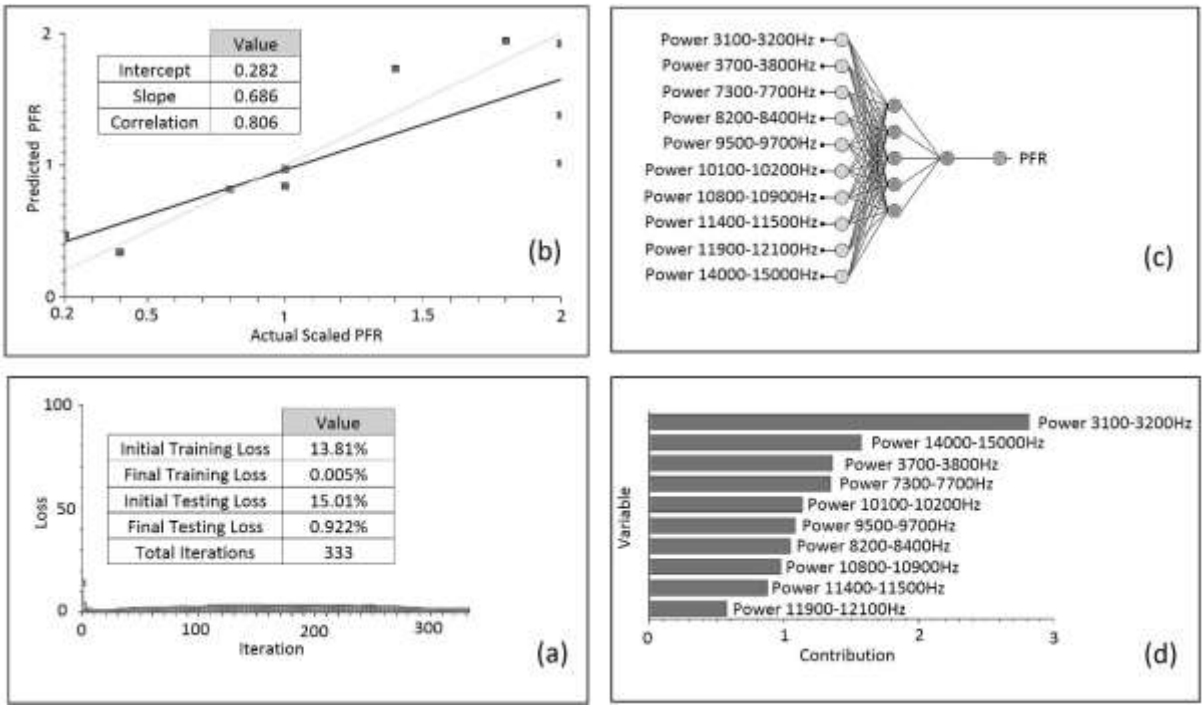

Figure 14. a) Error Calculations, b) Linear regression analysis, c) ANN architecture, d) Rating of input contribution to the outcome Powder Feed Rate (PFR) (Published Results [36])

To further assess the model accuracy, a standard linear regression analysis was carried out (**Figure 14.b**) between the scaled neural network outputs and the corresponding targets for the independent testing/validation subset and 3 parameters indicating the quality of the regression were calculated. The first two parameters correspond to the y-intercept and the slope of the best linear regression relating scaled outputs and targets. The third parameter is the correlation coefficient between the scaled outputs and the targets [35]. For a perfect fit (outputs exactly equal to targets), the slope would be 1, the y-intercept would be 0 and the correlation coefficient is equal to 1. **Figure 14.b** illustrates the linear regression for the scaled output Powder Feed Rate (PFR). The predicted values are plotted versus the actual ones as squares. The black line indicates the best linear fit (0.8 for this model). The grey line

indicates a perfect fit. A graphical representation of the network architecture is depicted in **Figure 14.c** The number of inputs is 10, and the number of outputs is 1 and the single hidden layer contains 5 neurons.

The dominant power peak frequencies that are highly correlated to PFR were determined without any information related to the SOD. For this reason, it is necessary to assess if the highly correlated frequencies remain linked to PFR when SOD dominated frequencies are introduced to the dataset. This task is executed by removing one input at a time. This shows which input has more influence in the selected output. **Figure 14.d** shows the importance of each input. If the importance takes a value greater than 1 for an input, it means that the testing/validation error without that input is greater than with it. In the case where the importance is lower than 1, the testing/validation error is lower without using that input. Finally, if the importance is 1, there is no difference between using the current input and not using it. The most important variable is the power peak at 3100-3200Hz range, that gets a contribution of 2.89 to the outputs followed by the peak power in the range of 14,000-15,000Hz with the second larger contribution of 1.57. The results confirm that high correlation is maintained when the dataset is jeopardised with irrelevant information (SOD in this case). Furthermore, the results are in line with the observations in section 6.1 suggesting that the powder feed rate would affect the jet shape promoting fast decay of the jet. The high frequency relates to the shear layer mixing and the low frequencies are affected by the large eddies at the jet core mixing region. As expected, the power change in mid frequency range is less important (contribution close to 1) when considering PFR alone.

4.2.2 Correlation ratios of SOD within the selected frequency bands

The same approach has been used to identify the correlation between the SOD and peak power frequencies when PFR related information are included in the neural Network. **Figure**

15.a illustrates the training strategy losses in each iteration. The initial value of the training loss was considerably lower at 0.0578946, and the final value after 3 iterations was 0.0578836. The initial value of the testing/validation loss was 0.0382135, and the final value after 3 iterations was 0.0382130. The training strategy was implemented sequentially resulting in a much faster network training. From the linear regression analysis (**Figure 15.b**) of the scaled standoff distance (SOD) output a better linear fit was achieved (0.95) indicating that the signals contain stronger information related to the spray distance as opposed to powder feed rates. The predictive neural network architecture was refined in order to minimize the model loss and is shown in **Figure 15.c.** The number of inputs is 10 and the number of outputs (SOD) is 1. The complexity, represented by the numbers of hidden neurons, is 7 and the architecture of this neural network can be written as 10:7:1. The size of the scaling layer is 10 and the scaling method used for this layer is the Mean Standard Deviation.

From the calculation of the testing/validation loss when removing one input at a time the most important variable is the peak power at 8200-8400Hz, that gets a contribution of 6.2 to the outputs. The results confirm that the strong correlation has been maintained after the inclusion of PFR related frequencies in the dataset. It is evident from **Figure 15.d** that the frequency range of interest has now moved to the low-mid frequency range as opposed to powder feed rate frequency range. The same has been observed in **Figure 13** where most power peak changes occur between 3,000-10,000Hz. Altering the position of the substrate opposite to the gun results in the creation of large vortex induced zones near the substrate. These large turbulent structures give rise to the low frequency power spectrum. This effect dominates over the upstream shear layer mixing noise.

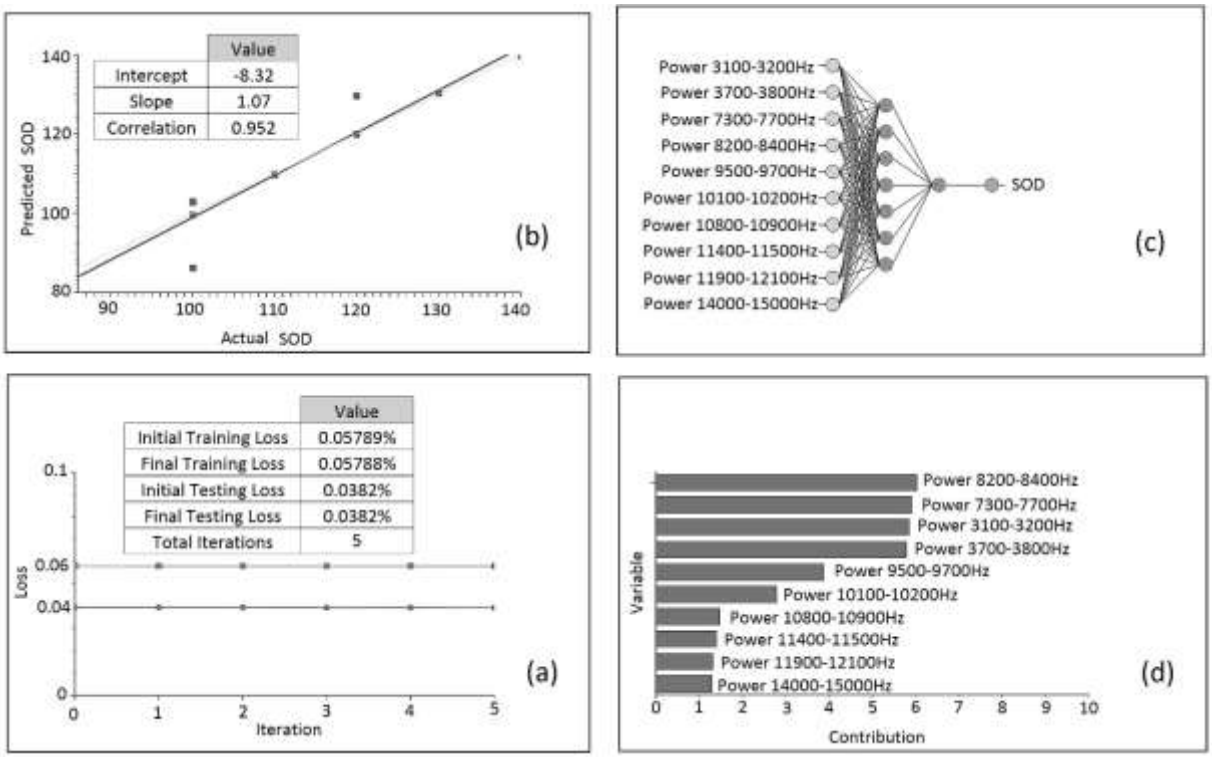

Figure 15. a) Error Calculations, b) Linear regression analysis, c) ANN architecture, d) Rating of input contribution to the outcome Stand-off distance (SOD) (Published Results [36])

4.2.3 Final ANN model accounting for combined influences on target microhardness

In the final stage we can reconstruct the target, which is the coating property, by introducing the microhardness data for all instances under study. The preliminary analysis demonstrated that the input power frequencies are highly correlated to selected targets (powder feed rate and SOD). These correlations occur over different frequency ranges indicating that these variables do not carry the same information and the ANN model shall benefit from their joint consideration. If the correlation rates were high over the same frequency range would mean that the PFR and SOD variables carry the same information from which the ANN model would not benefit introducing errors to the prediction of the coating microhardness when both spray inputs vary.

The linear regression parameter for the scaled output Coating Microhardness is illustrated in **Figure 16.a**. The intercept, slope and correlation are very similar to 0, 1 and 1, respectively, suggesting that the neural network is predicting the testing data well. The overall model accuracy is within 3% implying that in terms of coating microhardness the predictions may oscillate with a maximum deviation close to 30 HV0.3. The final number of layers in the neural network is 2 and the architecture of this neural network can be written as 10:3:1 as shown in **Figure 16.b**. The input importance analysis suggests that the most important input is in the range of 3100-3800Hz, that gets an average contribution of 3 to the outputs. This is the low frequency range mainly associated to large eddies and the impact of the jet on the substrate. As expected, the effect of SOD on the coating microhardness is known to be larger compared to the effect of small changes in the PFR.

The results suggest that there is strong combined influence when varying the SOD and PFR thus at least 10 frequency ranges should be monitored simultaneously in order to get accurate prediction of the coating microhardness during spray. This is more evident when examining how the outputs vary as a function of a single input, when all the others are fixed. This can be seen as the cut of the neural network model along some input direction and through some reference point. For the four predominant power peak frequencies the directional outputs are illustrated in **Figure 17**.

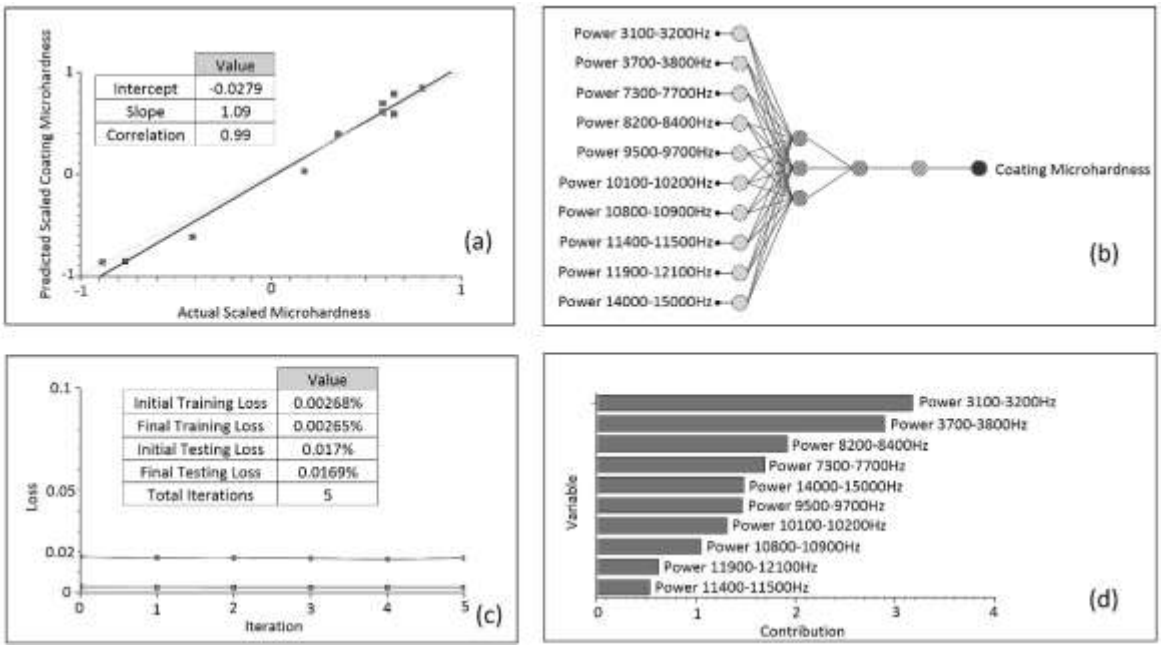

Figure 16. a) Linear regression analysis, b) ANN architecture, c) Error Calculations, d) Rating of input contribution to the outcome Coating Microhardness (HV0.3kg) (Published Results [36])

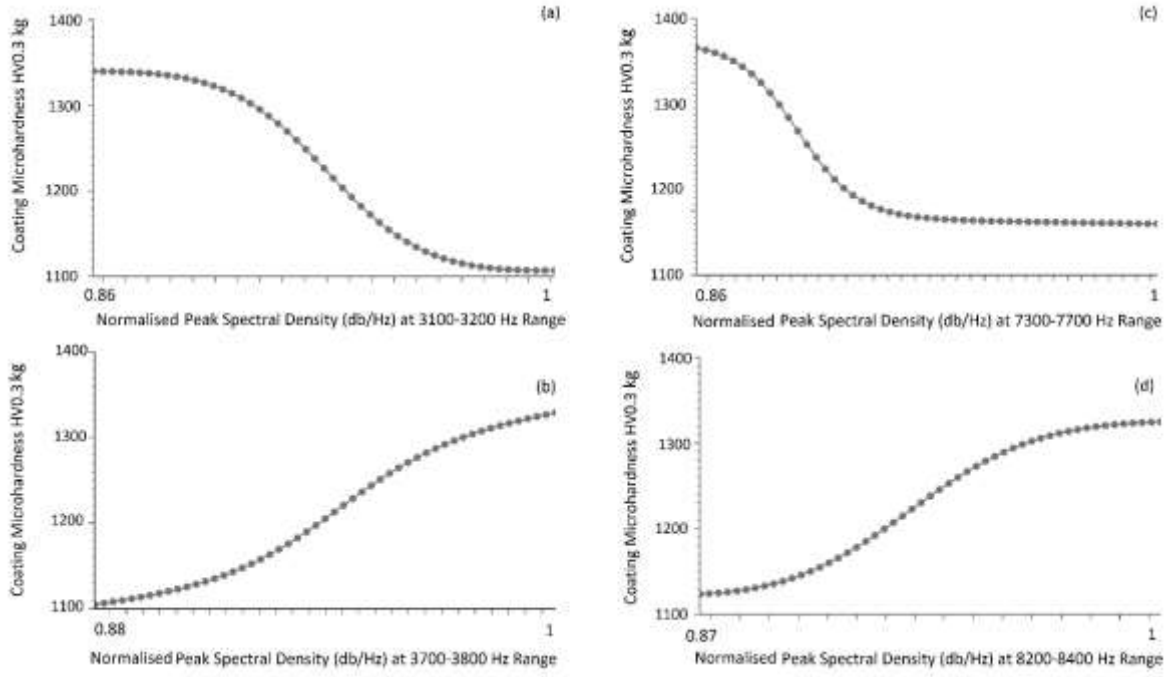

Figure 17. Variation of coating microhardness (HV0.3 kg) as a function of a single power frequency input. a) Signal power at 3100-3200 Hz, b) Signal power at 3700-3800 Hz, c) Signal power at 7300-7700 Hz, d) Signal power at 8200-8400 Hz (Published Results [36])

These plots show the output coating microhardness as a function of the input power at 3100-3200Hz, 3700-3800Hz, 8200-8400Hz and 7300-7700Hz. The x and y axes are defined by the range of peak power at a given frequency range and the coating microhardness respectively. For example, in the 3100-3200Hz range the high-power values indicate lower coating quality as opposed to the 8200-8400Hz range where coating quality increases with power. The resulting noise power levels contain information of both the PFR and the SOD which are not given as an input to the model. During spray, both parameters may change due to operational errors or as part of the spray process planning. For this reason, the predictive algorithm should be able to provide the key target output under any spray condition irrespectively.

The predictive ability of the developed ANN is further demonstrated in **Figure 17**. This is the inverse of the ANN architecture shown in **Figure 16.b**. The algorithm was tested against experimental data that were removed from the training dataset (unseen data). The single model input is the desired coating microhardness and the target values are the average power peaks in three dominant frequencies as described earlier. The powder feed rate was kept constant at 2 kg/h and the stand-off distance was fixed at 120mm. Very good agreement has been observed in all frequencies. The largest deviation from the experimental data was found at the lower frequency range where noisy data originate from the Rayleigh–Taylor instabilities that are responsible for the axisymmetric shedding of the jet. The accuracy and predictive capability of the model in unseen data is very promising and can pave the way for dynamic control of the process by iterative corrective intervention through the gas control unit and the robotic arm. This will require larger datasets and more advanced machine learning algorithms. Corrective actions may include increase or decrease of the gas flow rates, flame temperature control through stoichiometric ratio adaptations and adjustment of the SOD to achieve the desired acoustic power levels that lead to a desired coating property.

Similarly, the ANN model can be designed and trained to account for a single user input (for example a microhardness value) and multiple outputs (for example the SOD and PFR) to achieve the desired coating property as specified by the user.

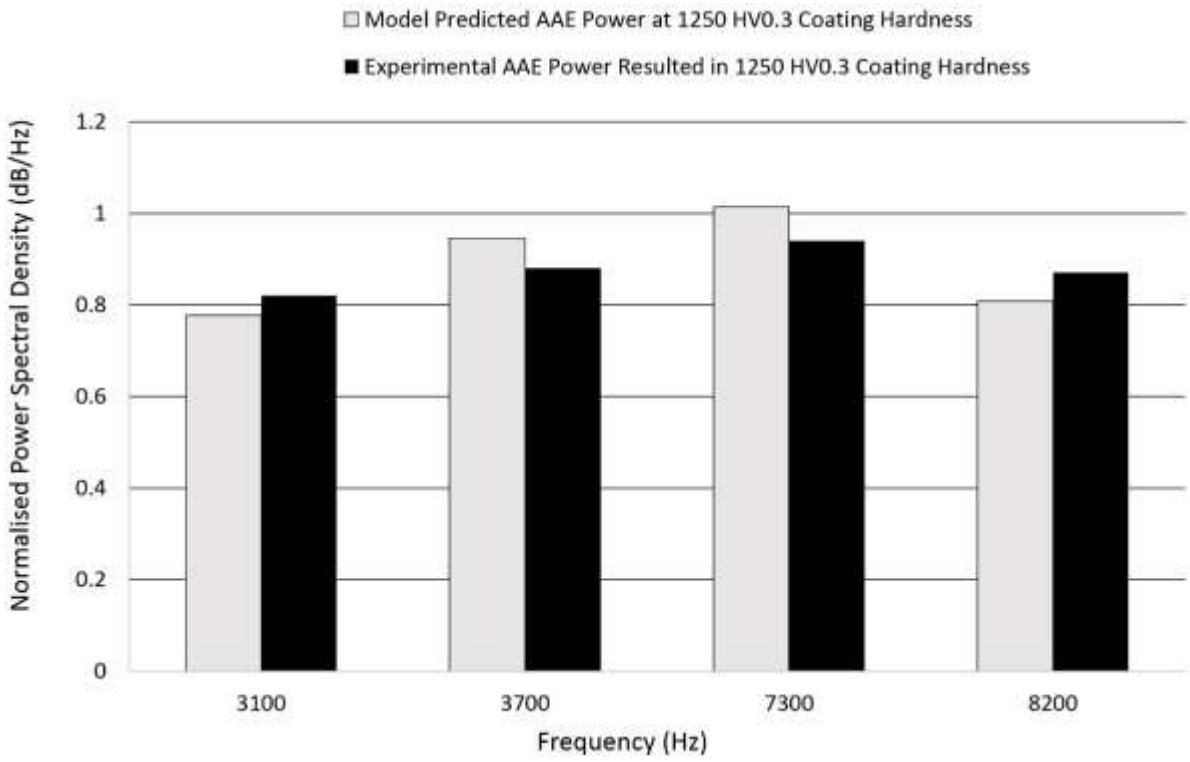

Figure 17. Unseen data predictive capability of the ANN. The spray distance was fixed at 120mm, the powder feed rate was 2kg/h, the traverse speed 600mm/s and the impact angle 90^{o}. (Published Results [36])

4.3 Conclusions

The main objective of the project was to demonstrate a methodology that could potentially lead to the design of a simple process monitoring device based on the airborne acoustic emissions generated during the HVOF or other high kinetic energy processes. The results demonstrate that intelligent sampling and QA monitoring linked to spray processing parameters is feasible. The work was executed in two main work packages. The first, placed increased emphasis on the numerical modelling of the HVOF process aeroacoustics. The modelling data confirmed the presence of unique detectable noise features that can be

attributed and correlated to several process variables, such as the powder feed rate and the stand-off distance. Most importantly, this work demonstrated that the information carried in the raw acoustic dataset contains process-variable specific signatures that an ANN can benefit from producing meaningful outputs. The second work package focused on raw data analysis and classification by implementing several cost effective shallow neural networks. Extensive error analysis and validation was carried out in order to finalise the model architecture. The ANN was trained using a relatively small experimental dataset; However, the input data were carefully selected and cleaned prior to ANN training. The generalisation and predictive capability of the model has been successfully assessed and validated. The authors hope that this work will motivate more research on intelligent airborne noise sampling as an alternative method that can offer improved QA and QC to our thermal spray community.

Chapter 5
Commercial Opportunities

5.1 Technology Impact in Potential Markets

These competitive times demand an easy to use solution to centrally monitor and manage quality-related operations across the enterprise. The proposed concept is a flexible system that makes quality management easier by connecting and automating quality related activities throughout an organization. Live and historic spray data will be available to a database enabling issues that affect quality to be quickly identified and resolved centrally—even across global operations and into the supplier network. Successful demonstration of the proposed technology will help manufacturers to efficiently meet the highest quality standards for delivered goods, reduce costs associated with poor quality, easily adapt and implement change, and drive operational excellence. The proposed technology will help large and medium organisations to globally leverage their application knowledge and optimize the services business by achieving business growth while improving profitability via increased utilizations and fostering operational excellence. The market this technology addressing has shown sustained growth over the last 20 years. Only in Europe there are more than 3000 mid-sized and small companies that produce thermal sprayed coatings with a total turnover estimated in almost 2 billion euros. Design for excellence and improved QA has a direct impact on the number of rejects annually (we estimate a reduction of 85%) which translates to approximately 5% savings for a spray company annually.

As the regulations concerning hard chrome plating (HCP) are getting more stringent and the variety of applications that benefit from thermal spray (TS) coatings is expanded, more sophisticated ways of monitoring and controlling the quality and process efficiency are

urgently needed. At the same time, there is an increasing interest in low temperature high kinetic energy thermal spray methods in order to avoid unwanted reactions in the deposited materials that occur in higher temperatures. The family of WC-Co hard metal coatings deposited via HVOF or HVAF outperform HCP and is the driving force behind this shift to lower deposition temperatures because they have established themselves as the leading successor of HCP. The new developed equipment will accelerate all optimization processes since the state of coating quality can be monitored in real time. Monitoring equipment will also allow the technicians to know when to replace the worn consumables of the thermal spraying gun, thus it will possible to optimize and to extend the life of the parts. By monitoring the particle impact "characteristics" it is also possible to readjust thermal spraying parameters of worn guns. At the moment, all spray monitoring systems are static and they cannot be used when the torch is in motion. So they can only provide stagnant diagnosis of the spray process which is rarely the case in commercial applications onto complex parts.

5.2 Market Analysis and Business Opportunity

Global thermal spray coating market size was estimated at USD 7.41 billion in 2014. Rising demand in various applications including automotive and aerospace is expected to be one of the key market drivers. Increasing application scope, owing to advantages such as wear and corrosion protection, low toxic gas emissions, thickness capability and electrical resistance is expected to fuel thermal spray coating market growth. However, low degree of adhesion on small substrates is expected to challenge industry growth over the next seven years. Key applications include aerospace precision parts, automotive, medical instruments and industrial gas turbines. Use of these coating for biomedical and medical instruments to improve wear resistance and boost biocompatibility of prosthetics and dental implants is expected to augment growth. Metal, ceramic, intermetallic and polymer are the most

prevalent products in the thermal spray coating industry. They are applied to various surfaces in order to achieve longer life spans under severe operating conditions. They are extensively used in manufacturing high strength low alloy steels for LPG tanks to prevent stress corrosion cracking. Expansion of the oil & gas industry particularly in North America and Middle East is expected to have a positive impact on demand over the forecast period. Increasing application scope in engineering coating, wear resistant coating, automotive & aerospace, biomedical, food processing, electronics, semiconductors and energy are further expected to promote demand. Shifting consumer trend from hard chrome to thermal spray in order to comply with stringent environmental standards particularly in Europe is expected to be one of the primary drivers. Technological upgradation to reduce overall cost is expected to be another key factor for growth over the next seven years.

Ceramics accounted for a significant share with revenue exceeding USD 2.20 billion in 2014. These are primarily employed in biomedical industry. HVOF technology is used to spray these products on to substrates which are further used in the medical sector for the manufacturing of dental implants. Expansion of this sector is expected to have a positive impact on growth over the next seven years Metals accounted for 22.4% share of the overall market in 2014. Wide range of microstructures, speed of coating deposition and feedstock flexibility make these coating a lucrative option for a use on metals and hence will be a key market driver over the next seven years. Stringent regulations by EPA and AFSP have led to the use of these products in automobile sector on account of increasing consumer safety and environment protection.

5.3 Quality Assurance

The quality control (QC) is generally considered as the rate limiting factor in the manufacturing environments when it comes to delivering the products on time. Most

commonly the coatings are tested in QC only after production is completed with the exception of raw material (RM) and in process quality control (IPQC). Most of the time, lots of samples are waited in queue to be tested. Lead time varies for test of sample of a product or group of products. The goal of reduced testing approach proposed in this project in QC lab is to use less effort, fewer resources and less time to test incoming samples. The in-line monitoring equipment is one of the next frontiers of the application of Operational Excellence (OE). When applied correctly the OE makes a great deal of sense by allowing the organizations to focus on testing that delivers quick, cost-effective results, enable better quality results, provide safer workplace and reduce frustrations. The operational excellence not only boosts the moral of the work force but also improves the lab efficiencies by doing reduced testing practices since the principles and techniques have been well proven.

References

N.H. Faisal, R. Ahmed, R.L. Reuben, and B. Allcock, AE Monitoring and Analysis of HVOF Thermal Spraying Process, *J. Therm. Spray Technol*., 2011, **20**(5), p 1071-1084

[2] H.A. Crostack, G. Reuss, T. Gath, and M. Dvorak, On-Line Quality Control in Thermal Spraying Using Acoustic Emission Analysis, Tagungsband Conference Proceedings, E. Lugscheider and R A. Kammer, Ed., March 17-19, 1999 (Düsseldorf, Germany), DVS Deutscher Verband für Schweißen, 1999, p 208-211

[3] E. Lugscheider, F. Ladru, H.A. Crostack, G. Reuss, and T. Haubold, On-line Process Monitoring During Spraying of TTBCs by Acoustic Emission Analyses, Tagungsband Conference Proceedings, E. Lugscheider and R A. Kammer, Ed., March 17-19, 1999 (Düsseldorf, Germany), DVS Deutscher Verband für Schweißen, 1999, p 312-317

[4] S. Nishinoiri, M. Enoki, and K. Tomita, In situ Monitoring of Microfracture During Plasma Spray Coating by Laser AE Technique, *Sci. Technol. Adv. Mater*., 2003, **4**(1), p 623-631

[5] Y. Wang, and P. Zhao, Noncontact Acoustic Analysis Monitoring of Plasma Arc Welding, *Int J Press Vessel Pip*, 2001, **78**(1), p 43–47

[6] W. Huang, and R. Kovacevic, (2009) Feasibility Study of Using Acoustic Signals for Online Monitoring of the Depth of Weld in the Laser Welding of High-Strength Steels, *Proc Inst Mech Eng B J Eng Manuf*, 2009, **223**(1), p 343–361

[7] E. Saad, H. Wang, and R. Kovacevic, Classification of Molten Pool Modes in Variable Polarity Plasma Arc Welding Based on Acoustic Signature, *J Mater Process Technol,* 2006,**174**(3), p 127–136

[8] L. Grad, J. Grum, I. Polajnar, and J. Marko Slabe, Feasibility Study of Acoustic Signals for On-line Monitoring in Short Circuit Gas Metal Arc Welding, *Int J Mach Tools Manuf*, 2004, **44**(5), p 555–561

[9] Y. Wang, Q. Chen, Z. Sun, and J. Sun, Relationship Between Sound Signal and Weld Pool Status in Plasma Arc Welding, *Trans Nonferrous Metals Soc Chin,* 2001, **11**(1), p 54–57

[10] W. Huang, and R. Kovacevic, A Neural Network and Multiple Regression Method for the Characterization of the Depth of Weld Penetration in Laser Welding Based on Acoustic Signatures, *J Intell Manuf*, 2011, **22**(2), p 131–143

[11] S. Kamnis, and S. Gu, Numerical Modelling of Propane Combustion in a High Velocity Oxygen–Fuel Thermal Spray Gun, *Chem. Eng. Process.*, 2006, **45**(4), p 246-253

[12] S. Kamnis, and S. Gu, 3-D Modelling of Kerosene-Fuelled HVOF Thermal Spray Gun, *Chem. Eng. Sci.,* 2006, **61**(16) p 5427-5439

[13] ANSYS Fluent 19, Academic Edition, ANSYS, inc., 2018

[14] J. E. Ffowcs-Williams, and D. L. Hawkings, Sound Generation by Turbulence and Surfaces in Arbitrary Motion, *Proc. Roy. Soc. London*, 1969, **264**(1), p 321–342

[15] J. Smagorinsky, General Circulation Experiments with the Primitive Equations. I. The Basic Experiment, *Month.Wea. Rev.*, 1963, **91**(1), p 99–164

[16]B. F. Magnussen and B. H. Hjertager., On Mathematical Models of Turbulent Combustion With Special Emphasis on Soot Formation and Combustion, *Symp. (Int..) Combust.*, 1976, 16(1), p 719-729

[17] S. Kamnis, S. Gu, T.J. Lu, and C. Chen, Computational Simulation of Thermally Sprayed WC–Co Powder, *Comput. Mater. Sci.*, 2008, **43**(4), p 1172-1182

[18] S. Gu, and S. Kamnis, Numerical Modelling of In-Flight Particle Dynamics of Non-Spherical Powder, *Surf. Coat. Technol.,* 2009, **203**(22), p 3485-3490

[19] A. D. Gosman, and E. Ioannides, Aspects of Computer Simulation of Liquid-Fuelled Combustors, *J. Energy*, 1983, **7**(6), p 482–490

[20] "Neural Networks Tutorial 3. Neural network", Artificial Intelligence Techniques Ltd., www.neuraldesigner.com/learning/tutorials/neural-network, 2019, Accessed 12 April 2017

[21] A. Pasini, Artificial Neural Networks for Small Dataset Analysis, *J. Thorac. Dis*., 2015, **7**(5), p 953-960

[22] K. Gurney, *An Introduction to Neural Networks*, Master e-book ed., UCL Press Ltd., 2004, Chap. 11

[23] A. Krenker, M. Volk, U. Sedlar, J. Bešter, A. Kos, Bidirectional Artificial Neural Networks for Mobile-Phone Fraud Detection, *ETRI Journal*., 2009, **31**(1), p. 92-94

[24] B. Kröse, P. Smagt, *An Introduction to Neural Networks*, 8th ed., The University of Amsterdam, 1996, Chap. 4

[25] R. Rojas, *Neural Networks: A Systematic Introduction*, Springer, 1st ed., 1996, Chap. 7

[26] J. Pulsford, S. Kamnis, J. Murray, M. Bai, T. Hussain, Effect of Particle and Carbide Grain Sizes on a HVOAF WC-Co-Cr Coating for the Future Application on Internal Surfaces: Microstructure and Wear, *J. Therm. Spray Technol*., 2018, **27**(5)., p 207-219

[27] V. Katranidis, S. Gu, B. Allcock, and S. Kamnis, Experimental Study of High Velocity Oxy-Fuel Sprayed WC-17Co Coatings Applied on Complex Geometries. Part A: Influence of Kinematic Spray Parameters on Thickness, Porosity, Residual Stresses and Microhardness, *Surf. Coat. Technol*., 2017, **311**(1), p 206-215

[28] V. Katranidis, S. Gu, T.R. Reina, E. Alpay, B. Allcock, and S. Kamnis, Experimental Study of High Velocity Oxy-Fuel Sprayed WC-17Co Coatings Applied on Complex Geometries. Part B: Influence of Kinematic Spray Parameters on Microstructure, Phase Composition and Decarburization of the Coatings, *Surf. Coat. Technol*., 2017, **328**(1), p 499-512

[29] "Diagnostic Electronics for Vibration Sensors VSE001", IFM Electronic Ltd. Kingsway Business Park, TW12 2HD, Great Britain, technical data, 2007

[30] S. Kamnis, Development of Multiphase and Multiscale Mathematical Models for Thermal Spray Process, Aston University, 2008.

[31] C. Yu, W.R. Wolf, R. Bhaskaran, and S.K. Le1e, Study of Noise Generated by a Tandem Cylinder Configuration Using LES and Fast Acoustic Analogy Formulations, AIAA Workshop in Aeroacoustics, 7-9 June 2010 (Stockholm, Sweden), AIAA, 2010

[32] M. Wang and P. Moin, Dynamic Wall Modelling for Large-Eddy Simulation of Complex Turbulent Flows, *Phys. Fluids*, 2002, **14**(7), p 2043-2051

[33] A.U. Zun, A.S. Lyrintizis, and G.A. Blaisdell, Coupling of Integral Acoustics Methods With LES for Jet Noise Prediction, *International Journal of Aeroacoustics*, 2005, **3**(4), p 297-346

[34] D.W. Bechert and B. Stahl, Excitation of Instability Waves in Free Shear Layers Part 2. Experiments, *J. Fluid Mech.,* 1988, **186**(1), p 63-84

[35] A. Pasini, V. Pelino, S. Potestà, A Neural Network Model for Visibility Nowcasting From Surface Observations: Results and Sensitivity to Physical Input Variables, *J Geophys Res,* 2001, **106**(14), p 951-9

[36] S. Kamnis, K. Malamousi, A. Marrs, K. Delibasis, Aeroacoustics and Artificial Neural Network of Airborne Acoustic Emissions During High Kinetic Energy Thermal Spraying, Journal of Thermal Spray Technology, May 2019